Momentum distribution of the uniform electron gas: Improved parametrization and exact limits of the cumulant expansion

Paola Gori-Giorgi[1,2] and Paul Ziesche[2]
[1]*INFM Center for Statistical Mechanics and Complexity, and Dipartimento di Fisica, Università di Roma "La Sapienza," Piazzale Aldo Moro 2, I-00185 Rome, Italy*
[2]*Max-Planck-Institut für Physik komplexer Systeme, Nöthnitzer Strasse 38, D-01187 Dresden, Germany*
(Received 19 July 2002; published 27 December 2002)

The momentum distribution of the unpolarized uniform electron gas in its Fermi-liquid regime, $n(k,r_s)$, with the momenta k measured in units of the Fermi wave number k_F and with the density parameter r_s, is constructed with the help of the convex Kulik function $G(x)$. It is assumed that $n(0,r_s), n(1^{\pm},r_s)$, the on-top pair density $g(0,r_s)$, and the kinetic energy $t(r_s)$ are known (respectively, from accurate calculations for $r_s = 1,\ldots,5$, from the solution of the Overhauser model, and from quantum Monte Carlo calculations via the virial theorem). Information from the high- and the low-density limit, corresponding to the random-phase approximation and to the Wigner crystal limit, is used. The result is an accurate parametrization of $n(k,r_s)$, which fulfills most of the known exact constraints. It is in agreement with the effective-potential calculations of Takada and Yasuhara [Phys. Rev. B **44**, 7879 (1991)], is compatible with quantum Monte Carlo data, and is valid in the density range $r_s \lesssim 12$. The corresponding cumulant expansions of the pair density and of the static structure factor are discussed, and some exact limits are derived.

DOI: 10.1103/PhysRevB.66.235116 PACS number(s): 71.10.Ca, 05.30.Fk

I. INTRODUCTION

In solid-state theory[1] and quantum chemistry,[2] the phenomenon of electron correlation and some of its details are hidden in the reduced densities and reduced density matrices[3–6] and their cumulants.[7,8] For the ground state of the uniform electron gas (jellium) of density $\rho = 3/(4\pi r_s^3)$ (in a.u.), these quantities are the pair density $g(x,r_s)$ and the momentum distribution $n(k,r_s)$, where k is measured in units of the Fermi wave number $k_F = (3\pi^2\rho)^{1/3}$ and x is the scaled interelectronic distance, $x = k_F r_{12}$.

Besides its relevance in the understanding of many effects in simple metals and semiconductors, the jellium model plays a crucial role in providing input quantities for approximate approaches to the many-electron problem of nonuniform density. Different approximate schemes, in fact, often need different quantities from jellium. As an example, density-functional theory (DFT) uses the exchange-correlation energy of the uniform electron gas for the widely used local-density approximation (LDA). For building nonempirical beyond-LDA functionals for use in DFT, the pair density of jellium is often needed.[9]

In such applications, the quantities from the uniform electron gas must be available in the form of analytic expressions. Since the jellium model is not exactly solvable, analytic expressions are built by interpolating between known exact limits, and by fitting the quantum Monte Carlo (QMC) data, when available. Relevant examples are (i) the correlation energy used in LDA implementation, built by using functional forms[10–12] that include exact limits, and interpolate the QMC data of Ceperley and Alder;[13] (ii) the pair density, built by combining exact properties and fitting to QMC data,[14,15] or by simply interpolating between exact limits;[16] (iii) the static local-field factor, parametrized by fitting[17] QMC data of the static response;[18] and (iv) the dynamical local-field factors, built by using many known exact constraints.[19] All these parametrized quantities are not strictly "exact," but are considered to be closest to the true quantities, in the sense that this is the best one can presently obtain, and in the sense that they are accurate enough for the purpose for which they are needed.

In recent years, there has been increasing interest in a particular approach to the many-electron problem of nonuniform density, the so-called density-matrix functional theory (DMFT) that uses the one-body density matrix as the basic variable.[6,20–22] Building a "local approximation" for DMFT is not an easy task. In a first attempt,[23] the momentum distribution $n(k,r_s)$ of jellium has been used as input. Besides this important application, for which a reliable parametrization of $n(k,r_s)$ is needed, there are other reasons to focus on the momentum distribution of jellium. The definitions of "exchange" and "correlation" in DMFT are different from those in DFT and in Hartree-Fock–like approaches. In DMFT, the cumulant part[7,8] of the pair density rises to be a key quantity. An accurate parametrization of $n(k,r_s)$ at metallic densities allows to extract the cumulant pair density of jellium, since the whole pair density is available.[14–16] The cumulant pair density can then be compared with recent attempts to calculate it in a high-density electron gas,[24,25] and can be diagonalized in terms of "cumulant geminals" (analog of "Overhauser geminals" for the pair density[26–28]). Also, the study of exact limiting behaviors of the cumulant pair density is of great interest, since some of these limits could be approximately valid in nonuniform systems.

The momentum distribution of the uniform electron gas is also useful for the calculation of the exchange-correlation correction to Compton profiles computed within LDA-DFT.[29] Note also that $n(k,r_s)$ determines the part of the local-field factor beyond the random-phase approximation (RPA) that takes into account the change in occupation

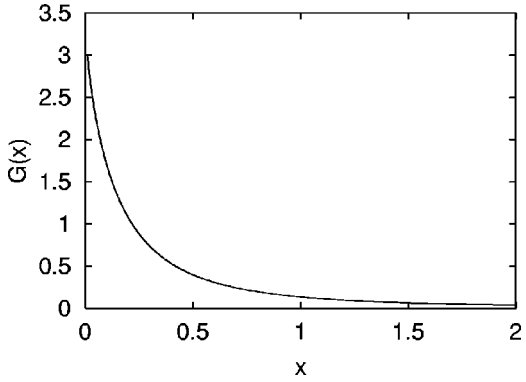

FIG. 1. The Kulik function $G(x)$ appearing in the RPA analysis of $n(k,r_s)$, see Eq. (A4). At the origin, $G(x)$ has a finite value, $G(0)=3.353\,337$ [Eq. (A7)], and a logarithmic-divergent slope, see Eq. (A6).

numbers in the Lindhard function [see Eq. (29) of Ref. 19].

The qualitative behavior of $n(k,r_s)$ is the following. It starts at $k=0$ with a value $n(0,r_s)\lesssim 1$, and decreases with increasing k. For $k<1$, it is concave. Then in the Fermi-liquid regime at $k=1$, there is a finite jump (Fermi gap) from $n(1^-,r_s)$ to a lower value $n(1^+,r_s)=n(1^-,r_s)-z_F(r_s)$ with logarithmic slopes at both sides of $k=1$. For $k>1$, (correlation tail) $n(k,r_s)$ is convex, and vanishes for $k\to\infty$. For $r_s=0$ (ideal Fermi gas), it is $n(k,0)=\theta(1-k)$, where $\theta(x)$ is the Heaviside step function. Thus, the quasiparticle weight $z_F(r_s)$ starts with $z_F(0)=1$, and decreases with increasing interaction strength r_s. At large r_s, the electrons form a Wigner crystal with a smooth $n(k,r_s)$. $r_s\ll 1$ and $r_s\gg 1$ are the weak- and strong-correlation limits, respectively. For intermediate values of r_s, a non-Fermi liquid regime may exist with $z_F=0$. In such case, $n(k,r_s)$ would be continuous vs k, with a nonanalytical behavior at $k=1$.

In Ref. 30, the idea of using the convex Kulik function $G(x)$ to parametrize the two branches ($k<1$ and $k>1$) of $n(k,r_s)$ is sketched. The function $G(x)$ appeared in Kulik's[31] RPA analysis of $n(k,r_s)$ near the Fermi edge ($|1-k|\ll 1$), see Eq. (A4). $G(x)$ behaves as $c_0+c_1 x\ln x$ for small x (see Appendix A and Fig. 1), which corresponds to the correct nonanalytic behavior of $n(k,r_s)$ near the Fermi surface. So, supposing that the value at the center, $n(0,r_s)$, and the values at the Fermi edge, $n(1^-,r_s)$ and $n(1^+,r_s)$, are known, it should be possible to represent $n(k,r_s)$ in terms of $G(x)$, with suitable prefactors and with suitable scaling (squeezing and stretching) of its argument. In this way, $n(k,r_s)$ becomes a functional of $n_0(r_s)=n(0,r_s)$, and of $n_\pm(r_s)=n(1^\pm,r_s)$, and can be designed to yield the proper normalization and the correct kinetic energy $t(r_s)$, which follows from the total energy $\epsilon(r_s)=t(r_s)+v(r_s)$ via the virial theorem.[32] In Ref. 30, the input data from Takada and Yasuhara (TY)[33,34] for $n_0(r_s)$, $n_\pm(r_s)$, and $t(r_s)$ at $r_s=1,\ldots,5$ have been used, together with the on-top pair density $g_0(r_s)=g(0,r_s)$ [which determines the large-k behavior of $n(k)$] from Ref. 27. The result is a field $n(k,r_s)$ for $r_s\in[1,6]$, which is correctly concave for $k<1$, convex for $k>1$, and with a Fermi gap $z_F(r_s)$ at $k=1$ decreasing with growing r_s. The attempt to extend this procedure for $r_s\in[6,10]$ failed; $n(k<1,r_s)$ is no longer concave for $r_s\gtrsim 6$.

Here, an improved version of the parametrization of $n(k,r_s)$ in terms of the Kulik function $G(x)$ is presented. Our parametrized momentum distribution is in good agreement with the TY values,[33,34] and is valid in the range of densities $r_s\lesssim 12$. Previous parametrizations of $n(k,r_s)$[35–38] used the QMC data of Ref. 35 as an input. However, QMC data are presently only available for $0.4\lesssim k\lesssim 0.9$ and $1.1\lesssim k\lesssim 1.5$, thus not providing information about $n(k,r_s)$ near the center, $k=0$, and at the Fermi edge, $k=1$. In these last regions, in fact, different parametrizations of the same QMC data can be rather different from each other.[35–37] Our construction of $n(k,r_s)$ uses information from the effective-potential calculations of Takada and Yasuhara,[33,34] from the high- and low-density limits of $n(k,r_s)$, corresponding to RPA and the Wigner crystal (WC) limit, and from accurate parametrizations of $t(r_s)$ (Ref. 12) and of $g_0(r_s)$.[27] In the regions where QMC data are available, our $n(k,r_s)$ is compatible with them. Also, with respect to previous works,[35–38] the functional form used here satisfies more exact limits. In particular, here the logarithmic behavior at the Fermi edge is taken into account.[39] Notice that it causes the logarithmic divergence of $t(r_s\to 0)$.[40]

Using our $n(k,r_s)$, the moments $\langle k^\nu\rangle$, the correlation entropy, and the one-body reduced density matrix $f(x,r_s)$ are evaluated. The latter appears in the cumulant partitioning of the pair density $g(x,r_s)$. The static structure factor $S(k,r_s)$, related to the pair density via Fourier transform, the particle-number fluctuations in fragments $\Delta N_\Omega(r_s)$, and the potential energy $v(r_s)$ are discussed in terms of their cumulant partitioning, and some exact limits are derived. Finally, by means of an accurate model for the spin-resolved pair density,[15] the cumulant part of $g(x,r_s)$ is extracted.

The paper is organized as follows. In Sec. II, the known sum rules and limiting cases for $n(k,r_s)$ are reported, and they are used in Sec. III to build up our parametrization of the momentum distribution via the Kulik function. Section IV is devoted to the calculation and discussion of different measures of the correlation strength, of the 1-matrix, and of the cumulant expansion of the pair density. In Sec. V, we study the cumulant partitioning of the static structure factor, of the density fluctuations, and of the potential energy. Conclusions and future developments are reported in Sec. VI.

II. SUM RULES AND LIMITING CASES

How is $n(k,r_s)$ defined? Starting from the many-body wave function $\Psi(1,\ldots,N)$, the one-body reduced density matrix (1-matrix for short) results from the $N-1$ contraction,

$$\gamma(1|1')=\int \frac{d2\cdots dN}{(N-1)!}\Psi(1,2,\ldots,N)\Psi^*(1',2,\ldots,N), \tag{1}$$

$$\int \frac{d1\cdots dN}{N!}|\Psi(1,\ldots,N)|^2=1,$$

with the notation $1\equiv(r_1,\sigma_1)$. For the uniform electron gas, $\gamma(1|1')=\rho\delta_{\sigma_1\sigma_1'}f(k_F|\bar{r}_1-r_1'|,r_s)$ defines the dimensionless 1-matrix $f(x,r_s)$. Then its Fourier transform is the momentum distribution

$$n(k,r_s)=\frac{\alpha^3}{2}\int_0^\infty dx^3\frac{\sin kx}{kx}f(x,r_s), \tag{2}$$

where $dx^3=3/4\pi\, d^3x=3x^2dx$ and $\alpha=(4/9\pi)^{1/3}$. $n(k,r_s)$ can be calculated using perturbation theory, directly with Green's functions,[31] see Figs. 1(a) and 1(b) of Ref. 24, or via the Hellmann-Feynman theorem[41] as the energy derivative $n(k,r_s)=\delta E/\delta\varepsilon_k$, supposed E is (perturbatively) known as a functional of $\varepsilon_k=\hbar k^2/2m$ and $v_q=4\pi e^2/q^2$.[42] Perturbative methods only work for high densities, $r_s\ll 1$. At metallic and lower densities, other techniques must be used, namely, the effective-potential method,[33] which combines perturbation theory (Green's functions) with the Fermi-hypernetted chain approach, and the QMC simulations.[35,43] A more complete list of references concerning calculations and parametrizations can be found in Ref. 30.

$n(k,r_s)$ has to satisfy the condition $0<n(k,r_s)<1$ (which guarantees the ensemble N-representability of the 1-matrix) and the sum rules (k in units of k_F, and energies in Ry)

$$\int_0^\infty dk^3 n(k,r_s)=1, \tag{3}$$

$$\frac{1}{(\alpha r_s)^2}\int_0^\infty dk^3 n(k,r_s)k^2=t(r_s), \tag{4}$$

where $t(r_s)$ can be written as the sum of the kinetic energy of the free Fermi gas, $3/5(\alpha r_s)^{-2}$, and of the kinetic energy of correlation, $t_{\rm corr}(r_s)$. For $r_s\ll 1$, $t_{\rm corr}(r_s)$ is known from RPA and from the lowest-order exchange diagram beyond it;[44–46] for a summary see Eq. (3.25) and Figs. 1(a) and 1(b) of Ref. 24. At larger r_s, $t_{\rm corr}(r_s)$ can be obtained via the virial theorem[32] from parametrized QMC correlation energies.[12] The large-k behavior of $n(k,r_s)$ is determined by the kinks in the many-body wavefunction, which occur whenever two electrons are at contact or ''on top'' (coalescing cusp properties),[47,48]

$$n(k\to\infty,r_s)=\frac{C(r_s)}{k^8}+O\left(\frac{1}{k^{10}}\right),$$

$$C(r_s)=\frac{8}{9\pi^2}(\alpha r_s)^2 g_0(r_s), \tag{5}$$

where $g_0(r_s)=g(0,r_s)$ is the on-top value of the pair-distribution function. In the $r_s\to 0$ limit, $g_0(r_s)$ can be obtained from perturbation theory,[49,50] and at larger r_s it has been calculated by solving an effective two-body Schrödinger equation.[27,51]

In a normal Fermi liquid,[52] the momentum distribution has a discontinuity and infinite slopes[53] at the Fermi edge, $k=1$,

$$n(k\to 1^-,r_s)=n_-(r_s)-A(r_s)(1-k)\ln(1-k)+O(1-k), \tag{6}$$

$$n(k\to 1^+,r_s)=n_+(r_s)+A(r_s)(k-1)\ln(k-1)+O(k-1). \tag{7}$$

In the following, $A(r_s)$ is referred to as the Fermi edge coefficient. In the small-r_s limit, $n_\pm(r_s)$ and $A(r_s)$ are known from RPA (see Appendix A). In the low-density or WC limit, the Fermi gap disappers $[n_-(r_s)\to n_+(r_s)]$, the infinite slopes at the Fermi edge may also vanish $[A(r_s)\to 0]$.

Near the center, $k\to 0$, $n(k,r_s)$ should behave quadratically,[36–38,43]

$$n(k\to 0,r_s)=n_0(r_s)+B(r_s)k^2+O(k^4). \tag{8}$$

A simple argument in favor of Eq. (8) is that it holds both in the high- and in the low-density limit (see Appendixes A and B).

When $r_s\to 0$, exact results for $n(k,r_s)$ are known by means of RPA[31,42] (Appendix A). In the RPA treatment, the Kulik function $G(x)$ appears,[31] see Eqs. (A3)–(A5) and Fig. 1. $G(x)$ will be used in the following section to build up a parametrized $n(k,r_s)$ that satifies Eqs. (3)–(8).

In the low-density or strongly correlated limit, $r_s\to\infty$, the electron gas undergoes Wigner crystallization (see, e.g., Refs. 54 and 56). A simple model for the momentum distribution in such regime is reported in Appendix B.

III. IMPROVED PARAMETRIZATION OF $n(k,r_s)$

The momentum distribution in terms of the Kulik function $G(x)$ of Fig. 1 is parametrized as follows. For $k<1$, we use the ansatz

$$n_<(k,r_s)=n_0-\frac{[n_0-n_-]}{G(0)}G[x_<(k,r_s)], \tag{9}$$

while for $k>1$ we use

$$n_>(k,r_s)=\frac{n_+}{G(0)}G[x_>(k,r_s)], \tag{10}$$

with $x_<(k,r_s)$ and $x_>(k,r_s)$ equal to

$$x_<(k,r_s)=a\frac{\alpha r_s}{2\pi^2}\frac{G(0)}{[n_0-n_-]}\frac{(1-k)}{\sqrt{4\alpha r_s/\pi}} + b\frac{\pi^2}{\alpha r_s}\sqrt{\frac{\pi}{3}\frac{(1-\ln 2)}{F''(0)}\frac{[n_0-n_-]}{G(0)}}\frac{(1-k)^2}{k}, \tag{11}$$

$$x_>(k,r_s)=a\frac{\alpha r_s}{2\pi^2}\frac{G(0)}{n_+}\frac{(k-1)}{\sqrt{4\alpha r_s/\pi}} + \sqrt{\frac{3\pi(1-\ln 2)}{g_0}\frac{n_+}{G(0)}}\frac{\pi}{4\alpha r_s}(k-1)^4. \tag{12}$$

Here $F''(0)=17.968\,746$ [see Appendix A, Eq. (A1)], and the r_s dependence of a, b, n_0, $n_\pm$, and g_0 is not explictly shown for shortness. These constructions are such that $n_<(k)\to n_0, n_-$ for $k\to 0,1^-$, respectively, and $n_>(k)\to n_+, 0$ for $k\to 1^+,\infty$, respectively. The behavior of the Kulik function for small and large arguments (see Appendix A) ensures the exact asymptotic expansion of Eqs. (5)–(8) near the center, near the Fermi surface, and for large k.

The parameter $a(r_s)$ determines the Fermi edge coefficient $A(r_s)$ of the $|1-k|\ln|1-k|$ term at the Fermi surface,

$$n(k\to 1^\pm, r_s)=n_\pm(r_s)\pm a(r_s)\left(\frac{\alpha r_s}{\pi}\right)^{1/2}\frac{1}{4}\left(\frac{\pi}{4}+\sqrt{3}\right)\times|1-k|\ln|1-k|+O(|1-k|). \tag{13}$$

The parameter $b(r_s)$ determines the curvature $B(r_s)$ of Eq. (8) at the center, $k=0$,

$$n(k\to 0, r_s)=n_0(r_s)-\frac{\pi^4}{\alpha^2}\frac{F''(0)}{2}\left[\frac{r_s}{b(r_s)}\right]^2 k^2+O(k^4). \tag{14}$$

For small r_s (RPA—see Appendix A), it is $a(r_s\to 0)=1$ and $b(r_s\to 0)=1$.

In the preliminary version of Ref. 30, another (but similar) ansatz was introduced, and it was chosen $b(r_s)=1$. Two different functions, $a_<(r_s)$ and $a_>(r_s)$, for the coefficient of $|1-k|\ln|1-k|$ at $k=1^-$ and $k=1^+$ were fixed by the sum rules of Eqs. (3) and (4) [with $t_{\rm corr}(r_s)$ from Ref. 12]. The values $n_0(r_s)$ and $n_\pm(r_s)$ were taken from the TY data (available for $r_s=1,\ldots,5$). The on-top value $g_0(r_s)$ was taken from Ref. 27.

In our improved ansatz of Eqs. (9)–(12), we set $a_<(r_s)=a_>(r_s)=a(r_s)$ (in agreement with Ref. 53; also Figs. 7 and 8 of Ref. 30 confirm this), and we use again $t_{\rm corr}(r_s)$ from Ref. 12 and $g_0(r_s)$ from Ref. 27. Since we want to extend our results in the density range $6\leqslant r_s\leqslant 10$, where there are no data available for $n_0(r_s)$ and $n_\pm(r_s)$, we extract information from the extreme low-density limit (Wigner crystal—see Appendix B) by following an oversimplified version of the idea presented in Ref. 55. We first build $n_0(r_s)$ by using a functional form that recovers the exact high-density limit, includes the Wigner crystal behavior as $r_s\to\infty$, and has some free parameters to be fitted to the TY data. The result is reported in Fig. 2, together with the high- and low-density curves. It is given by

$$n_0(r_s)=\frac{1+t_1 r_s^2+t_2 r_s^{5/2}}{1+t_3 r_s^2+t_4 r_s^{13/4}}, \tag{15}$$

with $t_1=0.003\,438\,169$, $t_2=0.007\,253\,136\,66$, $t_3=0.014\,900\,367$, $t_4=0.001\,132\,443\,64$ [t_1-t_3 agrees with the RPA value $-(\alpha/\pi^2)^2\,4.1123=-0.011\,46$]. We then build the parameter $b(r_s)$ by a simple interpolation between the high- and low-density limits of the curvature at the center (see Fig. 3). The result is

$$b(r_s)=(1+0.000\,937\,692\,5\,r_s^{13/4})^{1/2}. \tag{16}$$

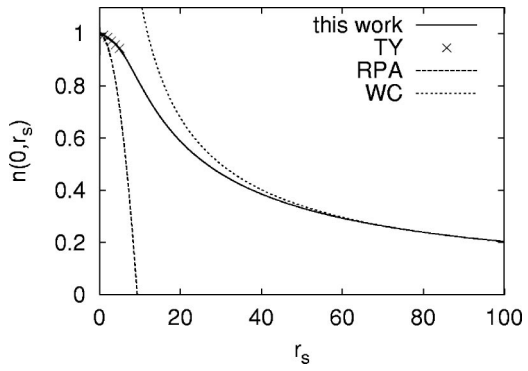

FIG. 2. Parametrized $n(0,r_s)$ (solid line), compared to the TY values (Refs. 33 and 34). The high-density or RPA limit and the WC limit are also shown.

Finally, the values at the Fermi edge, $n_\pm(r_s)$, and the coefficient of the infinite slope at the Fermi edge, $a(r_s)$, are obtained by fitting the TY values for $n_\pm(r_s)$ while imposing the normalization and the kinetic-energy[12] sum rules of Eqs. (3) and (4). The results are parametrized with the inclusion of the high- and low-density limits, and are equal to

$$n_-(r_s)=\frac{1+v_1 r_s+v_2 r_s^2+v_3 r_s^3}{1+v_4 r_s+v_5 r_s^2+v_6 r_s^3+v_7 r_s^{15/4}}, \tag{17}$$

with $v_1=-0.067\,979\,3$, $v_2=-0.001\,028\,46$, $v_3=0.000\,189\,111$, $v_4=0.020\,539\,7$, $v_5=-0.008\,683\,8$, $v_6=6.871\,09\times 10^{-5}$, $v_7=4.868\,047\times 10^{-5}$ [v_1-v_4 agrees with the RPA value $-(\alpha/2\pi^2)3.3533=-0.088\,519$], and

$$n_+(r_s)=\frac{q_1 r_s}{1+q_2 r_s^{1/2}+q_3 r_s^{7/4}}, \tag{18}$$

with $q_1=0.088\,519$ (from RPA), $q_2=0.45$, $q_3=0.022\,786\,335$;

$$a(r_s)=\frac{1+p_1 r_s^{1/4}+p_2 r_s^{1/2}}{1+p_3 r_s^{1/4}+p_4 r_s^{1/2}+p_5 r_s+p_6 r_s^6}, \tag{19}$$

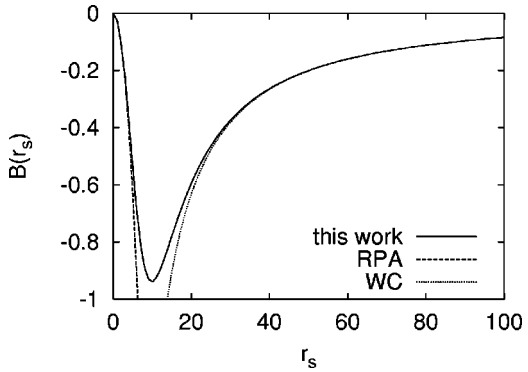

FIG. 3. Parametrized coefficient of the k^2 term near the center ($k\to 0$), $B(r_s)=-(\pi^4/\alpha^2)(F''(0)/2)[r_s/b(r_s)]^2$. The high-density or RPA result, $b(r_s\to 0)=1$, and the WC limit are also shown.

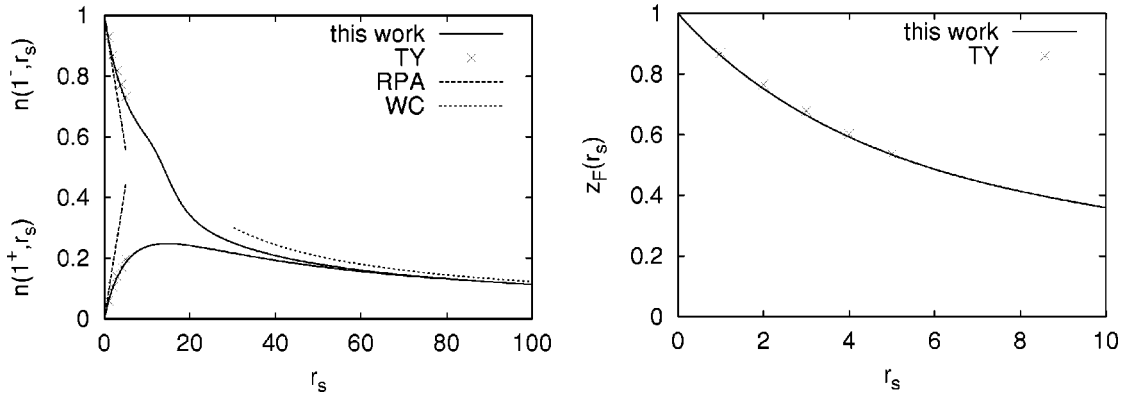

FIG. 4. Left panel: parametrized $n(1^{\pm},r_s)$ (solid lines), compared to the TY values (Refs. 33 and 34). The high-density or RPA limit and the WC limit are also shown. Right panel: value of the Fermi gap $z_F(r_s)=n(1^-,r_s)-n(1^+,r_s)$ as a function of r_s; the present parametrization is compared with the TY results (Refs. 33,34).

with $p_1=-78.8682$, $p_2=-0.098\,994\,1$, $p_3=-68.5997$, $p_4=38.1159$, $p_5=-17.6829$, and $p_6=-0.011\,367\,59$. Our parametrized $n(k,r_s)$ breaks down at $r_s\gtrsim 12$ [in the density range $12\lesssim r_s\lesssim 16$, $n(k>1,r_s)$ is no longer convex, and for $r_s\gtrsim 16$ the unphysical result $n_-<n_+$ is obtained when the sum rules of Eqs. (3) and (4) are imposed].

In the left panel of Fig. 4, we show the functions $n_{\pm}(r_s)$, together with the TY values, and the high- and low-density limits [here the $r_s\to\infty$ limit is considered to be the inflexion point of the WC momentum distribution, see Eq. (B4)]. As said, our model is only valid for $r_s\lesssim 12$, so that $n_-(r_s)$ and $n_+(r_s)$ at densities lower than $r_s=12$ are no more obtained from the constraints of Eqs. (3) and (4). Thus, the strange behavior of $n_-(r_s)$ at $r_s\sim 16$ does not affect our results. Also, the scheme presented here for the transition between the metallic and the extreme low-density region is oversimplified and must not be regarded as rigorous or reliable. We did not take into account the transition to the partially polarized electron gas (which affects the $r_s\gtrsim 50$ densities[56]) as well as many other features. However, our results seem to be reliable in the relevant density range $r_s\lesssim 12$, and the simple picture of the left panel of Fig. 4 is only a ''naive suggestion.'' In the right panel of Fig. 4, we compare our parametrized $z_F(r_s)$ with the TY results. In Fig. 5, we report the r_s dependence of the Fermi edge coefficient $A(r_s)$. Finally, in Fig. 6, we present in the left panel our parametrized $n(k,r_s)$ for $1\leqslant r_s\leqslant 10$, and in the right panel we compare our result with the TY $n(k,r_s)$ and with the QMC data of Ref. 35 for $r_s=5$.

IV. MOMENTS, CORRELATION ENTROPY, 1-MATRIX, AND CUMULANT EXPANSION

With the now available momentum distribution $n(k,r_s)$, its moments

$$\langle k^{\nu}\rangle=\int_0^{\infty} dk^3 n(k,r_s)k^{\nu} \tag{20}$$

can be evaluated in addition to the normalization for $\nu=0$ and the kinetic energy for $\nu=2$ [Eqs. (3) and (4)]. They are shown in Fig. 7 for $r_s=3$ and 10, together with the $r_s=0$ (ideal Fermi gas) and with the WC result ($r_s=75$). The expression

$$(\Delta t)^2=\frac{1}{(\alpha r_s)^4}[\langle k^4\rangle-\langle k^2\rangle^2] \tag{21}$$

(measured in Ry^2) describes the fluctuation of the kinetic energy. The moments $\langle k^2\rangle$ and $\langle k^4\rangle$ determine the small-x behavior of the 1-matrix, see Eq. (25). In Refs. 57 and 58, the entropylike expression $s(r_s)=-\langle \ln n(k,r_s)\rangle$ as a function of the interaction strength r_s has been used as a measure of the correlation strength.[59] Here the expression

$$s_{\mathrm{ph}}(r_s)=\int dk^3\,(-1)\{n(k,r_s)\ln n(k,r_s) + [1-n(k,r_s)]\ln[1-n(k,r_s)]\} \tag{22}$$

is introduced as an alternative with the understanding that $n(k,r_s)$ and $1-n(k,r_s)$ are the probabilities for the momentum state k to be occupied (with spin up and spin down) and empty, respectively. The entropy of this probability ''distribution'' is just the integrand of Eq. (22), and $s_{\mathrm{ph}}(r_s)$ is the sum of all these entropies. Notice its invariance under the

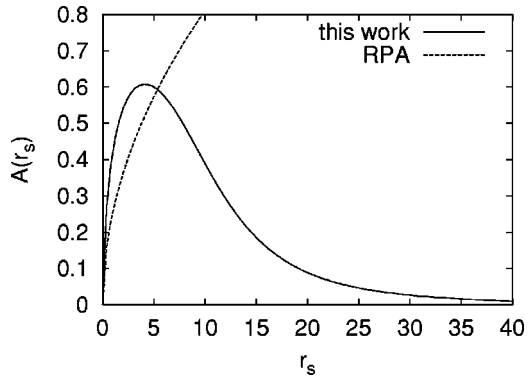

FIG. 5. Parametrized coefficient of the infinite slope at the Fermi edge, $A(r_s)=a(r_s)(\alpha r_s/\pi)^{1/2}0.63$. The present result is compared with the RPA value, $a(r_s\to 0)=1$. See Ref. 39.

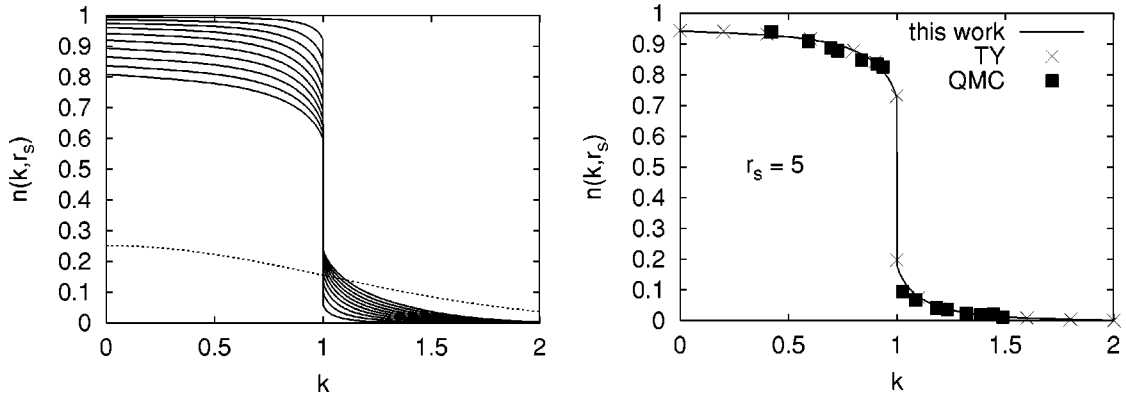

FIG. 6. Left panel: momentum distribution calculated with Eqs. (9)–(12) for $r_s=1,2,\ldots,10$ (solid lines). In the Wigner limit, $n(k,r_s \gg 1)$ is calculated with Eq. (B1) (dashed line, corresponding to $r_s=75$). Right panel: comparison of the present work with the TY (Refs. 33,34) momentum distribution and the QMC calculation of Ref. 35 for $r_s=5$.

exchange $n(k,r_s)\leftrightarrow 1-n(k,r_s)$, which is referred to as particle-hole symmetry in the reduced-density-matrix community. This symmetry is an intrinsic property of the correlation energy as a functional of the 1-matrix.[61] $s_{\rm ph}(r_s)$ is plotted in Fig. 8. Another measure of the correlation strength is the correlation-tail normalization

$$n_{\rm corr\ tail}(r_s)=\int_1^\infty dk^3\, n(k,r_s), \tag{23}$$

also reported in Fig. 8. For large r_s, the Fermi edge disappears, $z_{\rm F}(r_s)=0$ [and also any relict of it, $A(r_s)=0$], then the inflexion point of $n(k,r_s)$ vs k may serve in Eq. (23) as the lower limit.

With $n(k,r_s)$ also, the (dimensionless) 1-matrix,

$$f(x,r_s)=\int_0^\infty dk^3 \frac{\sin kx}{kx} n(k,r_s), \quad x=k_{\rm F}|\underline{r}-\underline{r}'|, \tag{24}$$

is available as the inverse of Eq. (2). It has the small-x behavior,

$$f(x\ll 1,r_s)=1-\frac{\langle k^2\rangle}{3!}x^2+\frac{\langle k^4\rangle}{5!}x^4-\frac{1}{5!}\frac{2}{9\pi}(\alpha r_s)^2 g_0(r_s)x^5 + O(x^6), \tag{25}$$

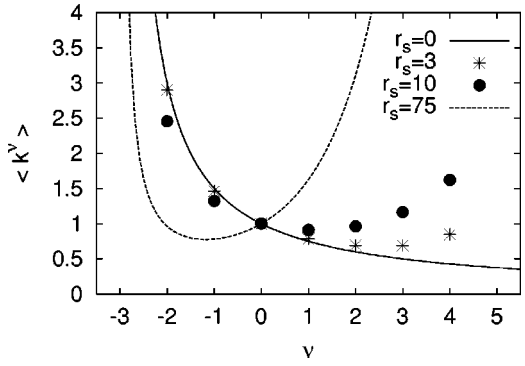

FIG. 7. The moments $\langle k^\nu\rangle$ of $n(k,r_s)$ for $r_s=3$ and $r_s=10$. The corresponding results for the noninteracting gas ($r_s=0$) and for the Wigner crystal at $r_s=75$ are also reported.

and the large-x asymptotics (Friedel oscillations with reduced amplitudes),

$$f(x\gg 1,r_s)=-3\, z_{\rm F}(r_s)\frac{\cos x}{x^2} + \frac{3}{x^3}[z_{\rm F}(r_s)\sin x-\pi A(r_s)\cos x]+O\left(\frac{1}{x^4}\right), \tag{26}$$

see Appendix C. $A(r_s)=a(r_s)(\alpha r_s/\pi)^{1/2}0.63$ is the Fermi edge coefficient, the prefactor of the logarithmic term $(k-1)\ln|k-1|$ in $n(k\approx 1,r_s)$. The factor 0.63 is the Kulik number 7.91, see Eq. (A6), divided by 4π. In the inverse Fourier transform (2), the oscillatory terms of Eq. (26) do not affect the small-k behavior of $n(k,r_s)$, because their average is zero. Since $n(k\ll 1,r_s)=n_0(r_s)+O(k^2)$, the large-$x$ behavior of the nonoscillatory $f(x,r_s)$ is $\propto 1/x^6$ or faster. $f(x,r_s)$ is displayed in Fig. 9. One may partition $n(k,r_s)$, and correspondingly $f(x,r_s)$, in the following way:

$$n(k,r_s)=z_{\rm F}(r_s)\,\theta(1-k)+n_1(k,r_s),$$

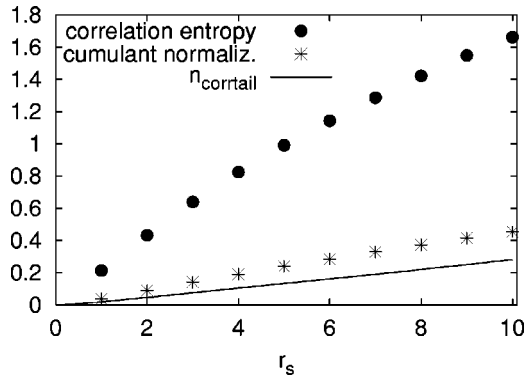

FIG. 8. The particle-hole symmetric correlation entropy [Eq. (22)], the normalization of the cumulant pair density [right-hand side(rhs) of Eq. (34)], and the correlation tail normalization $n_{\rm corr\ tail}(r_s)$ [Eq. (23)] as a function of r_s.

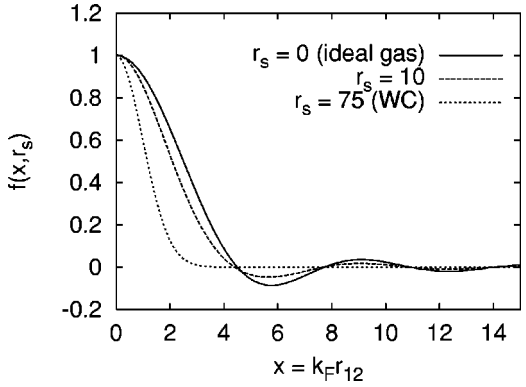

FIG. 9. 1-matrix $f(x,r_s)$ for $r_s=0$ (ideal Fermi gas), for $r_s=10$ (present model), and for $r_s=75$ [WC limit, Eq. (B1)].

$$f(x,r_s)=3\,z_{\mathrm{F}}(r_s)\frac{j_1(x)}{x}+f_1(x,r_s), \tag{27}$$

where $j_1(x)=(\sin x-x\cos x)/x^2$. $n_1(k,r_s)$ is a continuous function with $n_1(1^-,r_s)=n_1(1^+,r_s)$ and an infinite slope at $k=1$. Figure 10 shows $n_1(k,r_s)$ and $f_1(x,r_s)$ for $r_s=5$.

The 1-matrix squared appears in the cumulant partitioning of the pair density,

$$g(x,r_s)=1-\frac{1}{2}|f(x,r_s)|^2-h(x,r_s),\quad x=k_{\mathrm{F}}r_{12}. \tag{28}$$

This defines the cumulant pair density $h(x,r_s)$, which is the diagonal of the cumulant 2-matrix $\chi(1|1',2|2')$. The spin-resolved version of Eq. (28) is

$$g_{\uparrow\uparrow}(x,r_s)=1-|f(x,r_s)|^2-h_{\uparrow\uparrow}(x,r_s),$$

$$g_{\uparrow\downarrow}(x,r_s)=1-h_{\uparrow\downarrow}(x,r_s), \tag{29}$$

with $g(x,r_s)=\frac{1}{2}[g_{\uparrow\uparrow}(x,r_s)+g_{\uparrow\downarrow}(x,r_s)]$ and $h(x,r_s)=\frac{1}{2}[h_{\uparrow\uparrow}(x,r_s)+h_{\uparrow\downarrow}(x,r_s)]$. Notice that the (generalized exchange or) Fock term $|f(x,r_s)|^2$ appears only in the parallel-spin pair density and not in the antiparallel-spin pair density. $g_{\uparrow\uparrow}(x,r_s)$ describes the Fermi hole (due to both Pauli and Coulomb repulsion) with $g_{\uparrow\uparrow}(0,r_s)=h_{\uparrow\uparrow}(0,r_s)=0$, and $g_{\uparrow\downarrow}(x,r_s)$ describes the Coulomb hole (only due to the Coulomb repulsion) with $g(0,r_s)<1$. In addition to the above-mentioned correlation-strength indices, the quantities $h''_{\uparrow\uparrow}(0,r_s)$ measuring the on-top Fermi-hole curvature, and $h_{\uparrow\downarrow}(0,r_s)$ measuring the on-top Coulomb hole are other ones.

From Eq. (26), it follows

$$|f(x\gg 1,r_s)|^2=\frac{9}{2}\left[\frac{z_{\mathrm{F}}^2(r_s)}{x^4}+\frac{2\pi A(r_s)z_{\mathrm{F}}(r_s)}{x^5}\right](1+\cos 2x)$$
$$-9\frac{z_{\mathrm{F}}^2(r_s)}{x^5}\sin 2x+O\left(\frac{1}{x^6}\right). \tag{30}$$

If this is inserted into Eq. (28), then the nonoscillatory terms,

$$\frac{9}{2}\frac{z_{\mathrm{F}}^2}{x^4}+\frac{9\pi z_{\mathrm{F}}A}{x^5},$$

are canceled by the asymptotics of $h(x,r_s)$, which follow from the sum-rule properties of the static structure factor $S(q,r_s)$, see Sec. V and Ref. 52. The nominator of the oscillating $1/x^5$ term can be written as

$$9z_{\mathrm{F}}\sqrt{z_{\mathrm{F}}^2(r_s)+\pi^2A^2(r_s)}\cos(2x+2x_0(r_s)),$$

$$\tan 2x_0(r_s)=\frac{z_{\mathrm{F}}(r_s)}{\pi A(r_s)}.$$

The on-top properties of $g_{\uparrow\uparrow}(x\ll 1,r_s)$ and $g_{\uparrow\downarrow}(x\ll 1,r_s)$ are determined by the coalescing cusp theorems.[47,62]

With Eq. (29), with the spin-resolved pair densities of Ref. 15, and with $f(x,r_s)$ of this paper, the resulting cumulant pair densities $h_{\uparrow\uparrow}(x,r_s)$ and $h_{\uparrow\downarrow}(x,r_s)$ are plotted in Fig. 11. For small r_s ($\ll 1$), our results agree with those of Ref. 24.

V. STATIC STRUCTURE FACTOR, DENSITY FLUCTUATIONS, AND POTENTIAL ENERGY

The cumulant partitioning of Eq. (28) causes corresponding decompositions of all the quantities containing $1-g(x,r_s)$. Such quantities are the static structure factor $S(q,r_s)$, the fluctuation $\Delta N_\Omega(r_s)$ of the particle number in a

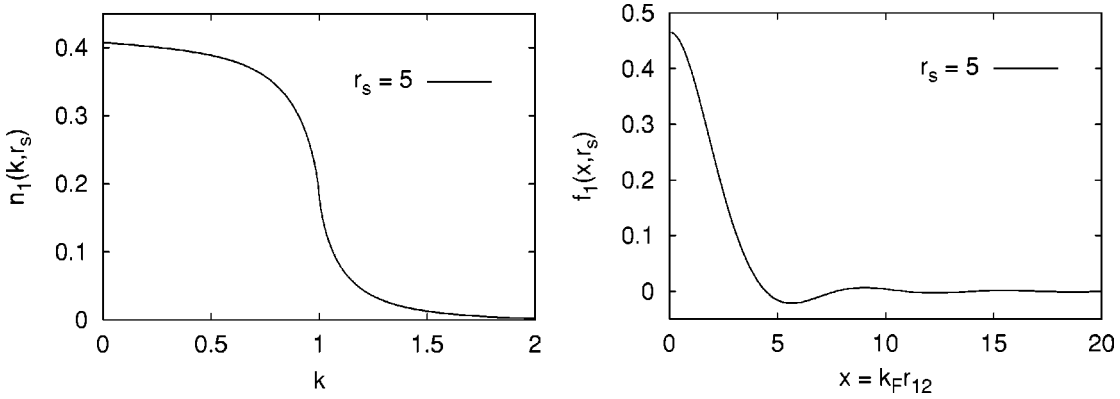

FIG. 10. Continuous part of $n(k,r_s)$, $n_1(k,r_s)=n(k,r_s)-z_{\mathrm{F}}(r_s)\theta(1-k)$ (left panel), and the corresponding 1-matrix $f_1(x,r_s)$ (right panel). The oscillations of $f_1(x)$ are due to the infinite slope of $n_1(k)$ at $k=1$.

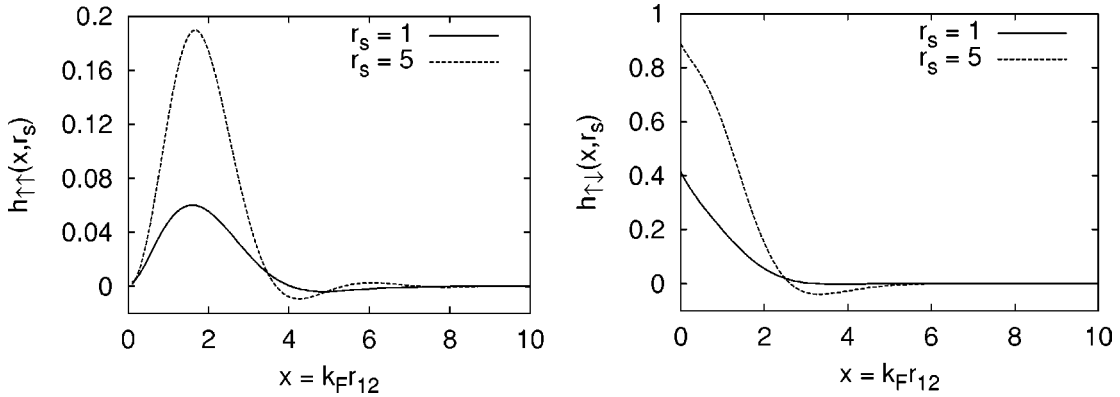

FIG. 11. Cumulant pair densities for parallel and antiparallel spins, obtained by combining the present work with the results of Ref. 15.

fragment Ω, and the potential energy $v(r_s)$.

So, the static structure factor is given by

$$S(q,r_s)=1-\frac{1}{2}\tilde{n}^2(q,r_s)-\tilde{h}(q,r_s), \tag{31}$$

with the (generalized exchange or) Fock component

$$\tilde{n}^2(q,r_s)=\alpha^3\int_0^\infty dx^3\frac{\sin qx}{qx}|f(x,r_s)|^2$$
$$=\int_0^\infty dk^3 n(k,r_s)\int_{-1}^{+1}d\zeta\, n(\sqrt{k^2+q^2-2kq\zeta},r_s), \tag{32}$$

[from which it follows that $\tilde{n}^2(q,r_s)$ has a discontinuity in its second derivative at $q=2$], and the cumulant component

$$\tilde{h}(q,r_s)=\alpha^3\int_0^\infty dx^3\frac{\sin qx}{qx}h(x,r_s), \tag{33}$$

which is simply the Fourier transform of the cumulant pair density $h(x,r_s)$. In Eq. (32) the convolution theorem has been applied. $\tilde{n}^2(q,r_s)$ is related to the probability of finding a pair of electrons with given relative momentum q.[27,28]

Notice that the sum rule $S(q\to 0,r_s)=0$ is equivalent to the sum rule

$$\alpha^3\int_0^\infty dx^3 h(x,r_s)=\int_0^\infty dk^3 n(k,r_s)[1-n(k,r_s)]. \tag{34}$$

The left-hand side (lhs) equals $\tilde{h}(0,r_s)$ and the rhs equals $1-\frac{1}{2}\tilde{n}^2(0,r_s)$. Löwdin had asked what meaning the rhs has.[63] According to Eq. (34), it fixes the normalization of the cumulant pair density $h(x,r_s)$ and is another particle-hole symmetric measure of the correlation strength; it is also reported in Fig. 8. Equation (34) is sometimes called perfect screening sum rule or charge neutrality condition.

For noninteracting electrons ($r_s=0$), the cumulant part vanishes, $\tilde{h}(q,r_s)=0$, and the Fock part $S_F(q,r_s)$ simply yields

$$S_0(q)=\frac{q}{2}\left[\frac{3}{2}-\frac{1}{2}\left(\frac{q}{2}\right)^2\right]\theta\left(1-\frac{q}{2}\right)+\theta\left(\frac{q}{2}-1\right), \tag{35}$$

with the linear small-q behavior $3q/4$. For interacting electrons ($r_s\neq 0$), the small-q sum rule[52,64]

$$S(q\ll 1,r_s)=\frac{1}{2(\alpha r_s)^2\omega_{\rm pl}(r_s)}q^2+O(q^4), \tag{36}$$

and the large-q sum rule[62]

$$S(q\gg 1,r_s)=1-\frac{8}{3\pi}\alpha r_s g_0(r_s)\frac{1}{q^4}+O\left(\frac{1}{q^6}\right) \tag{37}$$

hold. $\omega_{\rm pl}^2(r_s)=4\pi e^2\rho/m=3/r_s^3$ a.u. defines the plasma frequency.

The nonidempotency and the singularities of $n(k,r_s)$ determine the small-q behavior of $S_F(q,r_s)=1-\frac{1}{2}\tilde{n}^2(q,r_s)$,

$$S_F(q\ll 1,r_s)=S_F(0,r_s)+\frac{3}{4}z_F^2(r_s)q-A(r_s)z_F(r_s)$$
$$\times q^2\ln q+O(q^2), \tag{38}$$

as shown in Appendix D. Notice that $S_F(0,r_s)$ is equal to the rhs of Eq. (34). In Fig. 12, we report $S_F(q,r_s)$ for the

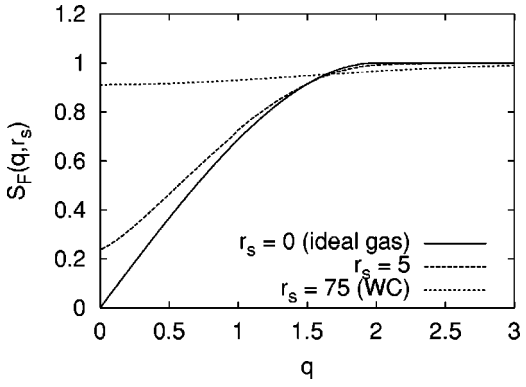

FIG. 12. The Fock component of the static structure factor for $r_s=0$ (ideal Fermi gas), $r_s=5$ (present work), and in the WC limit for $r_s=75$.

ideal gas ($r_s=0$), for $r_s=5$, and in the WC limit.

Equation (38), together with the sum rule of Eq. (36), allows to extract the large-x behavior of $h(x,r_s)$. Namely, because of Eq. (36), $\tilde{h}(q,r_s)$ must cancel both the linear and the $q^2\ln q$ terms of $\tilde{n}^2(q,r_s)$. This implies that the large-x behavior of the oscillation-averaged $\langle h(q,r_s)\rangle$ is

$$\langle h(x\gg 1,r_s)\rangle = -\frac{9}{4}\frac{z_F^2(r_s)}{x^4} - \frac{9}{2}\frac{\pi A(r_s) z_F(r_s)}{x^5} + O\left(\frac{1}{x^6}\right). \tag{39}$$

In Eq. (28) these terms cancel with the nonoscillatory long-range part of $\frac{1}{2}|f(x,r_s)|^2$.

If we consider within the uniform electron gas a certain fragment Ω (e.g., a sphere of radius R) containing on average $N_\Omega=\Omega/(4\pi r_s^3/3)=(R/r_s)^3$ electrons, and ask for the particle-number fluctuation ΔN_Ω, then the answer is[65,66]

$$\begin{aligned}\frac{(\Delta N_\Omega)^2}{N_\Omega} &= 1-\frac{(\alpha r_s)^6}{N_\Omega}\int_\Omega d^3x_1\int_\Omega d^3x_2 \\ &\quad\times\left[\frac{1}{2}|f(x,r_s)|^2+h(x,r_s)\right] \\ &= 1-\frac{(\alpha r_s)^6}{N_\Omega}\frac{3}{8\pi} \\ &\quad\times\int d^3q\left|\int_\Omega d^3x e^{i\underline{q}\underline{x}}\right|^2\left[\frac{1}{2}\tilde{n}^2(q,r_s)+\tilde{h}(q,r_s)\right], \\ x &= |\underline{x}_1-\underline{x}_2|. \end{aligned} \tag{40}$$

Again one may ask how differently the Fock and the cumulant parts contribute to their sum and to the conclusion "correlation suppresses fluctuations."[1,66] In the case of a sphere $\Omega=4\pi R^3/3$, the term in the modulus in Eq. (40) is just $\Omega 3j_1(qR)/(qR)$, so that the Fock term yields

$$\left[\frac{(\Delta N_\Omega)^2}{N_\Omega}\right]_F = 1-\frac{3}{2}\pi^2\Omega(\alpha r_s)^9\int_0^\infty dq^3\left[\frac{3\,j_1(qR)}{qR}\right]^2\tilde{n}^2(q,r_s). \tag{41}$$

Also, the potential energy $v(r_s)$ consists of a Fock and a cumulant part:[7]

$$\begin{aligned} v(r_s) &= -\frac{\alpha^2}{r_s}\int_0^\infty dx^3\left[\frac{1}{2}|f(x,r_s)|^2+h(x,r_s)\right]\frac{1}{x} \\ &= -\frac{\alpha^2}{r_s}\frac{3}{2}\int_0^\infty dq^3\left[\frac{1}{2}\tilde{n}^2(q,r_s)+\tilde{h}(q,r_s)\right]\frac{1}{q^2} \end{aligned} \tag{42}$$

(in Ry). The Fock part can also be written as[7]

$$\begin{aligned} v_F(r_s) &= -\frac{3}{2\pi\alpha r_s}\int_0^\infty dk\, n(k,r_s)\int_0^\infty dk' n(k',r_s) \\ &\quad\times kk'\ln\frac{k+k'}{|k-k'|}. \end{aligned} \tag{43}$$

In lowest order, with $n(k,r_s)\to\theta(1-k)$, Eq. (43) yields $-3/(2\pi\alpha r_s)$. The logarithmic term of $v(r_s\to 0)$ arises from $v_C(r_s)$, not from $v_F(r_s)$.[24]

VI. SUMMARY AND OUTLOOK

In Ref. 30, it was shown that the convex Kulik function $G(x)$, with appropriate prefactors and with an appropriate inhomogeneous scaling of its argument, reproduces the momentum distribution $n(k,r_s)$ of the unpolarized uniform electron gas of density $\rho=3/4\pi r_s^3$ in the metallic-density regime $r_s\in[1,6]$. The r_s functions $n(0,r_s)$, $n(1^\pm,r_s)$, the on-top pair density $g(0,r_s)$, and the kinetic energy $t(r_s)$ form the input for such construction. In this work, we improved the parametrization of $n(k,r_s)$ via the Kulik function, and we extended it up to $r_s\lesssim 12$, including the high-density regime [Eqs. (9)–(12) and Fig. 6].

The Fourier transform of $n(k,r_s)$ yields the one-body reduced density matrix $f(x,r_s)$ (Figs. 9 and 10), with large x oscillations arising from the Fermi gap $z_F(r_s)$ and the Fermi edge coefficient $A(r_s)$, the prefactor of the logarithmic term in $n(k\approx 1,r_s)$, which is included in our parametrization (Fig. 5). Several measures of the correlation strength have been discussed (Fig. 8). With reliable models for the pair density $g(x,r_s)$, the cumulant pair density $h(x,r_s)=1-\frac{1}{2}|f(x,r_s)|^2-g(x,r_s)$ has been extracted (Fig. 11) as a prestep of its diagonalization in terms of cumulant geminals (analog with the diagonalization of the pair density in terms of Overhauser geminals). Future work also includes the generalization to the partially polarized gas. In this case, with $\zeta=(N_\uparrow-N_\downarrow)/N$, one has to consider different cases. For spin polarization ζ between 0 and 1, two momentum distributions are to be described, $n_\uparrow(k,r_s,\zeta)$ for the spin-up electrons and $n_\downarrow(k,r_s,\zeta)$ for the spin-down electrons. So far, only the input data $g_0(r_s,\zeta)$ (Ref. 27) and $t(r_s,\zeta)$ (Ref. 12) are available in this more general case.

A small FORTRAN subroutine, which numerically evaluates our parametrized $n(k,r_s)$, is available at http://axtnt2.phys.uniroma1.it/PGG/elegas.html.

ACKNOWLEDGMENTS

The authors thank Y. Takada for providing the data for $n(0,r_s)$ and $n(1^\pm,r_s)$, and J. Cioslowski and G. Diener for helpful discussions. One author (P.G.-G.) gratefully aknowledges hospitality at the Max-Planck-Institut für Physik komplexer Systeme of Dresden (Germany); the other author (P.Z.) thanks P. Fulde for supporting this work.

APPENDIX A: RANDOM-PHASE APPROXIMATION

In RPA, it is[31,42] $n(k,r_s)=1-(\alpha r_s/\pi^2)^2H(k,1)$ for $k<1$ and $(\alpha r_s/\pi^2)^2H(k,1)$ for $k>1$, where

$$H(x<1,y)=\frac{1}{x}\left\{\int_{1-x}^{1+x}\frac{dq}{q}\int_0^\infty du\left[\frac{\frac{1-x^2}{2q}}{\left(\frac{1-x^2}{2q}\right)^2+u^2}-\frac{\frac{q}{2}+x}{\left(\frac{q}{2}+x\right)^2+u^2}\right]\frac{Q(q,u)}{q^2+y\frac{\alpha r_s}{\pi^2}Q(q,u)}\right.$$

$$\left.+\int_{1+x}^\infty\frac{dq}{q}\int_0^\infty du\left[\frac{\frac{q}{2}-x}{\left(\frac{q}{2}-x\right)^2+u^2}-\frac{\frac{q}{2}+x}{\left(\frac{q}{2}+x\right)^2+u^2}\right]\frac{Q(q,u)}{q^2+y\frac{\alpha r_s}{\pi^2}Q(q,u)}\right\},$$

$$H(x>1,y)=\frac{1}{x}\int_{x-1}^{x+1}\frac{dq}{q}\int_0^\infty du\left[\frac{\frac{x^2-1}{2q}}{\left(\frac{x^2-1}{2q}\right)^2+u^2}-\frac{x-\frac{q}{2}}{\left(x-\frac{q}{2}\right)^2+u^2}\right]\frac{Q(q,u)}{q^2+y\frac{\alpha r_s}{\pi^2}Q(q,u)},$$

and

$$Q(q,u)=2\pi\left\{1+\frac{1+u^2-q^2/4}{2q}\ln\frac{(1+q/2)^2+u^2}{(1-q/2)^2+u^2}-u\left[\arctan\frac{1+q/2}{u}+\arctan\frac{1-q/2}{u}\right]\right\}.$$

For small or large k (far from the Fermi edge) it is $H(k,1)\to F(k)$ with $F(k)=H(k,0)$. $F(k)$ has the small and large k properties,

$$F(k\ll 1)=4.112\,335+8.984\,373k^2+O(k^4) \tag{A1}$$

and

$$F(k\gg 1)=\frac{8\pi^2}{9}\frac{1}{k^8}+O\left(\frac{1}{k^{10}}\right), \tag{A2}$$

respectively.[20,21] The coefficient of $1/k^8$ is 8.772 98. For k near the Fermi edge, it is[20,21]

$$H(k,1)\to\frac{\pi^2}{2\alpha r_s}\frac{1}{k^2}G\left(\frac{|k-1|}{\sqrt{4\alpha r_s/\pi}}\right), \tag{A3}$$

with

$$G(x)=\int_0^\infty du\,\frac{R'(u)}{R(u)}\,\frac{u}{u+y}\,\frac{R(u)-R(y)}{u-y}\bigg|_{y=x/\sqrt{R(u)}} \tag{A4}$$

and

$$R(u)=1-u\arctan\frac{1}{u}. \tag{A5}$$

$G(x)$ has the small-x behavior,[31]

$$G(x\ll 1)=G(0)+\left[\pi\left(\frac{\pi}{4}+\sqrt{3}\right)x+O(x^2)\right]\ln x+O(x), \tag{A6}$$

with

$$G(0)=\int_0^\infty du(-1)\frac{R'(u)}{R(u)}\arctan\frac{1}{u}\approx 3.353\,337. \tag{A7}$$

The coefficient of $x\ln x$ is 7.908 799 (the Kulik number). $G(x)$ has the large-x behavior,

$$G(x\gg 1)=\frac{\pi}{6}(1-\ln 2)\frac{1}{x^2}+O\left(\frac{1}{x^4}\right). \tag{A8}$$

The coefficient of $1/x^2$ is 0.160 668 (the Macke number). The Kulik function $G(x)$ is shown in Fig. 1.

APPENDIX B: THE MOMENTUM DISTRIBUTION OF THE WIGNER CRYSTAL

In the low-density (large r_s) or strongly correlated limit, the electrons localize[54] and form a ferromagnetic body-centered-cubic lattice with an electrostatic (or Madelung) energy of $-1.792/r_s$ Ry.[67] The next term, $+2.65/r_s^{3/2}$ Ry, describes the coupled harmonic zero-temperature motion in lowest order.[68–70] To estimate the corresponding $n(k,r_s)$, we define with $3\hbar\omega/2=2.65/r_s^{3/2}$ (in Ry, or $\omega=0.88/r_s^{3/2}$ in a.u.) the frequency of indepent oscillating electrons (Einstein model). So, from the momentum distribution of the harmonic-oscillator ground state, it follows

$$n(k,r_s\to\infty)=\frac{4\pi}{3}\frac{1}{(\pi\omega/k_F^2)^{3/2}}e^{-k^2/(\omega/k_F^2)}; \tag{B1}$$

see Refs. 71–73, p. 19. Note that k is dimensionless (measured in units of k_F), and that $\omega/k_F^2=0.88\alpha^2 r_s^{1/2}=0.24r_s^{1/2}$. In Ref. 72, the factor 1 is used instead of 0.88. $n(k,r_s\to\infty)$ is correctly normalized and yields with Eq. (4) the kinetic energy (in Ry)

$$t(r_s\to\infty)=\frac{1}{2}\frac{2.65}{r_s^{3/2}}+\cdots, \tag{B2}$$

as it should. The corresponding potential energy is

$$v(r_s\to\infty)=-\frac{1.792}{r_s}+\frac{1}{2}\frac{2.65}{r_s^{3/2}}+\cdots. \tag{B3}$$

The inflexion-point trajectory with r_s as parameter is described by (see left panel of Fig. 4)

$$k_{\rm infl}(r_s)=[\omega/(2k_{\rm F}^2)]^{1/2}=0.35r_s^{1/4},$$

$$n_{\rm infl}(r_s)=\frac{4\pi}{3}\frac{e^{-1/2}}{(\pi\omega/k_{\rm F}^2)^{3/2}}=\frac{3.88}{r_s^{3/4}}. \tag{B4}$$

The region $k>k_{\rm infl}$ (to be referred to as correlation tail) contributes to the normalization the constant amount

$$\int_{k_{\rm infl}}^{\infty}dk^3n(k,r_s)=\mathrm{erf}\left(\frac{1}{\sqrt{2}}\right)-\sqrt{\frac{2}{\mathrm{e}\pi}}=0.80. \tag{B5}$$

From Eq. (B1), it follows for $n(0,r_s\to\infty)$,

$$n_0(r_s\to\infty)=\frac{4}{3\pi^{1/2}}\left(\frac{1}{0.24r_s^{1/2}}\right)^{3/2}=\frac{6.40}{r_s^{3/4}}, \tag{B6}$$

see Fig. 2; and for the curvature at the center (the coefficient of k^2),

$$-\frac{4}{3\pi^{1/2}}\frac{1}{(0.88\alpha^2r_s^{1/2})^{5/2}}=-\frac{26.71}{r_s^{5/4}}, \tag{B7}$$

see Fig. 3.

A more refined treatment takes into account that in harmonic approximation there are two transversal branches of harmonic lattice vibrations, $\omega_{t_{1,2}}(\underline{q},r_s)$, and one longitudinal branch $\omega_l(\underline{q},r_s)$ in the face-centered cubic Brillouin zone, satisfying the sum rule $\omega_{t_1}^2(\underline{q},r_s)+\omega_{t_2}^2(\underline{q},r_s)+\omega_l^2(\underline{q},r_s)=\omega_{\rm pl}^2(r_s)$. For $q=0$, it is $\omega_{t_{1,2}}(0,r_s)=0$, and therefore $\omega_l(0,r_s)=\omega_{\rm pl}(r_s)$. But also in this case the virial theorem holds, and assuming that $n(k,r_s)$ is a Gaussian distribution, then Eq. (B1) turns out again.

APPENDIX C: 1-MATRIX NEAR THE DIAGONAL AND FAR FROM IT

The equation $\gamma(1|1')=\rho\,\delta_{\sigma_1\sigma_1'}f(k_{\rm F}|\underline{r}_1-\underline{r}_1'|)$ defines the dimensionless 1-matrix $f(x)$. Its small-x behavior of Eq. (25) follows from the large-k behavior of $n(k)$ [Eq. (5)]. Namely, with $\sin y/y=1-(y^2/3!)+(y^4/5!)-\cdots$, and with the integrability of $n(k)k^2k^\nu$ for $\nu=0,\ldots,4$, it is

$$f^{(\nu)}(0)=\int_0^\infty dk^3n(k)k^\nu\left(\frac{d}{dy}\right)^\nu\frac{\sin y}{y}\Big|_{y=0}, \tag{C1}$$

which yields the first three terms of Eq. (25). Here $f^{(\nu)}(0)=(d/dx)^\nu f(x)|_{x=0}$.

Since $n(k)k^2k^5$ is nonintegrable, one has to compute $f^{(5)}(0)$ with the Kimball procedure,[62,74] which defines by using

$$n(k)=\frac{C}{(1+k^2)^4}+\mathcal{N}(k),\quad C=\frac{8}{9\pi^2}(\alpha r_s)^2g_0(r_s), \tag{C2}$$

a stronger (namely, $\sim 1/k^{10}$ for $k\to\infty$) decaying function $\mathcal{N}(k)$, so that $\mathcal{N}(k)k^2k^5$ is now integrable, yielding 0 because of $(d/dy)^5\sin y/y|_{y=0}=0$. Thus,

$$f^{(5)}(0)=\left(\frac{d}{dy}\right)^5p(x)|_{x=0}, \tag{C3}$$

with

$$p(x)=C\int_0^\infty\frac{dk^3}{(1+k^2)^4}\frac{\sin kx}{kx}=C\frac{\pi}{32}(3+3x+x^2)\mathrm{e}^{-x}. \tag{C4}$$

It follows

$$f^{(5)}(0)=-C\frac{\pi}{4}=-\frac{2}{9\pi}(\alpha r_s)^2g_0(r_s), \tag{C5}$$

Q.E.D.

The large-x behavior (26) follows from Eq. (24) by partial integration. Thereby the discontinuities of $n(k,r_s)$ at $k\approx 1$ appear. They determine the amplitudes of the Friedel oscillations:

$$f(x,r_s)=-z_{\rm F}(r_s)\frac{3\cos x}{x^2}+z_{\rm F}(r_s)\frac{3\sin x}{x^3}+f_1(x,r_s), \tag{C6}$$

with

$$f_1(x\gg 1,r_s)=-A(r_s)\frac{3}{x^3}\left\{\left[\frac{\pi}{2}+\mathrm{Si}(x)\right]\cos x-\mathrm{Ci}(x)\sin x\right\}$$
$$+O\left(\frac{1}{x^4}\right)=-A(r_s)\pi\frac{3\cos x}{x^3}+O\left(\frac{1}{x^4}\right). \tag{C7}$$

$z_{\rm F}(r_s)$ is the Fermi gap and $A(r_s)$ is the Fermi edge coefficient.

APPENDIX D: FOCK COMPONENT OF THE STATIC STRUCTURE FACTOR AT SMALL q

According to the definition of Eq. (32), the oscillations of $|f(x\gg 1,r_s)|^2$ [see Eq. (30)] only affect the discontinuities in

$\tilde{n}^2(q,r_s)$ and in its derivatives at $q=2$, while the small-q behavior of $\tilde{n}^2(q,r_s)$ is only affected by the oscillation-averaged part of $|f(x,r_s)|^2$, i.e., by

$$\langle f^2(x\gg 1,r_s)\rangle = \frac{9}{2}\frac{z_{\rm F}^2(r_s)}{x^4} + 9\frac{\pi A(r_s) z_{\rm F}(r_s)}{x^5} + O\left(\frac{1}{x^6}\right). \tag{D1}$$

Following the procedure of Kimball,[62,74] we define a function $\mathcal{F}(x)$ by

$$\langle f^2(x,r_s)\rangle = \mathcal{F}(x) + \frac{9}{2}\frac{z_{\rm F}^2(r_s)}{(1+x^2)^2} + 9\frac{\pi A(r_s) z_{\rm F}(r_s)}{(1+x)^5}, \tag{D2}$$

so that $\mathcal{F}(x\to\infty)\propto 1/x^6$. Then, the second term will give the coefficient of the linear term in $\tilde{n}^2(q,r_s)$, while the third term will give the coefficient of a term $\propto q^2\ln q$. By carrying out the calculations, one obtains Eq. (38), Q.E.D.

[1] P. Fulde, *Electron Correlation in Molecules and Solids* (Springer, Berlin, 1995).

[2] R. J. Bartlett, *Chemistry for the 21st Century* (Wiley, Weinheim, 2001), p. 271.

[3] E. R. Davidson, *Reduced Density Matrices in Quantum Chemistry* (Academic Press, New York, 1976).

[4] R. Erdahl and V. H. Smith, Jr., *Density Matrices and Density Functionals* (Reidel, Dordrecht, 1987).

[5] A. J. Coleman and V. I. Yukalov, *Reduced Density Matrices* (Springer, Berlin, 2000).

[6] J. Cioslowski, *Many Electron Densities and Reduced-Density Matrices* (Kluwer/Plenum, New York, 2000).

[7] P. Ziesche, Solid State Commun. **82**, 597 (1992).

[8] P. Ziesche, in *Many Electron Densities and Reduced-Density Matrices* (Ref. 6), p. 33.

[9] J. P. Perdew, in *Electronic Structure of Solids '91*, edited by P. Ziesche and H. Eschrig (Akademie Verlag, Berlin, 1991); J.P. Perdew, K. Burke, and M. Ernzerhof, Phys. Rev. Lett. **77**, 3865 (1996); **78**, 1396 (1997).

[10] S.H. Vosko, L. Wilk, and M. Nusair, Can. J. Phys. **58**, 1200 (1980).

[11] J.P. Perdew and A. Zunger, Phys. Rev. B **23**, 5048 (1981).

[12] J.P. Perdew and Y. Wang, Phys. Rev. B **45**, 13 244 (1992).

[13] D.M. Ceperley and B.J. Alder, Phys. Rev. Lett. **45**, 566 (1980).

[14] J.P. Perdew and Y. Wang, Phys. Rev. B **46**, 12 947 (1992); **56**, 7018 (1997).

[15] P. Gori-Giorgi, F. Sacchetti, and G.B. Bachelet, Phys. Rev. B **61**, 7353 (2000); **66**, 159901(E) (2002).

[16] P. Gori-Giorgi and J.P. Perdew, Phys. Rev. B **66**, 165118 (2002).

[17] M. Corradini, R. Del Sole, G. Onida, and M. Palummo, Phys. Rev. B **57**, 14 569 (1998).

[18] S. Moroni, D.M. Ceperley, and G. Senatore, Phys. Rev. Lett. **69**, 1837 (1992); **75**, 689 (1995).

[19] C.F. Richardson and N.W. Ashcroft, Phys. Rev. B **50**, 8170 (1994).

[20] J. Cioslowski, P. Ziesche, and K. Pernal, Phys. Rev. B **63**, 205105 (2001).

[21] J. Cioslowski, P. Ziesche, and K. Pernal, J. Chem. Phys. **115**, 8725 (2001).

[22] J. Cioslowski, K. Pernal, and P. Ziesche, J. Chem. Phys. **117**, 9560 (2002).

[23] K. Yasuda, Phys. Rev. Lett. **88**, 053001 (2002).

[24] P. Ziesche, Int. J. Quantum Chem. **90**, 342 (2002).

[25] P. Ziesche, in *Electron Correlations and Materials Properties II*, edited by A. Gonis, N. Kioussis, and M. Ciftan (Kluwer/Plenum, New York, in press).

[26] A.W. Overhauser, Can. J. Phys. **73**, 683 (1995).

[27] P. Gori-Giorgi and J.P. Perdew, Phys. Rev. B **64**, 155102 (2001).

[28] B. Davoudi, M. Polini, R. Asgari, and M.P. Tosi, Phys. Rev. B **66**, 075110 (2002); In a subsequent paper [cond-mat/0206456 (unpublished)], the same authors go beyond the Hartree-like theory and show how the inclusion of exchange let emerge liquidlike structures with increasing coupling strength r_s through the formation of a first-neighbor shell and further oscillations in the PD $g(x,r_s)$.

[29] L. Lam and P.M. Platzman, Phys. Rev. B **9**, 5122 (1974); G.E.W. Bauer, *ibid.* **27**, 5912 (1983); G.E.W. Bauer and J.R. Schneider, Phys. Rev. Lett. **52**, 2061 (1984); A. Görling, M. Levy, and J.P. Perdew, Phys. Rev. B **47**, 1167 (1993); S. Huotari *et al.*, *ibid.* **66**, 085104 (2002).

[30] P. Ziesche, Phys. Status Solidi B **232**, 231 (2002).

[31] I.O. Kulik, Zh. Éksp. Teor. Fiz. **40**, 1343 (1961) [Sov. Phys. JETP **13**, 946 (1961)].

[32] N.H. March, Phys. Rev. **110**, 604 (1958).

[33] Y. Takada and H. Yasuhara, Phys. Rev. B **44**, 7879 (1991).

[34] Y. Takada (private communication), on the basis of the method described in Ref. 33.

[35] G. Ortiz and P. Ballone, Phys. Rev. B **50**, 1391 (1994); **56**, 9970 (1997).

[36] G. Senatore, S. Moroni, and D.M. Ceperley, in *Physics of Strongly Coupled Plasmas*, edited by W.D. Kraeft (World Scientific, Singapore, 1995).

[37] B. Barbiellini and A. Bansil, J. Phys. Chem. Solids **62**, 2181 (2001).

[38] B. Farid, V. Heine, G.E. Engel, and I.J. Robertson, Phys. Rev. B **48**, 11 602 (1993).

[39] The infinite slope at the Fermi edge was previously taken into account in a study of the momentum distribution of ^{3}He (Ref. 45); the authors also extracted the Fermi edge coefficient A of Eqs. (6) and (7) from QMC simulations. At the equilibrium density, they found $A=0.06(2)$.

[40] J. Cioslowski (private communication).

[41] H. Hellmann, *Einführung in die Quantenchemie* (Deuticke, Leipzig, 1937), pp. 61 and 285. The original Russian version is G. Gel'man, *Quantenchemie* (ONTI, Moscow, 1936), p. 428; R.P. Feynman, Phys. Rev. **56**, 340 (1939). What usually is referred to as Hellmann-Feynman theorem has been first formulated by P. Güttinger, Z. Phys. **73**, 169 (1932), see Eq. (11). This

result is already implicitly contained in Eq. (28) of M. Born and V. Fock, *ibid.* **51**, 165 (1928). Whereas in these papers any parameter is considered, Hellmann and later Feynman explicitly referred to the special case of nuclear coordinates within the Born-Oppenheimer approximation, leading to the ''Hellmann-Feynman'' forces upon nuclei. Within perturbation theory, the theorem was already given by E. Schrödinger, Ann. Phys. (Leipzig) **80**, 437 (1926). Thus the theorem is due to Schrödinger, Born, Fock, Güttinger, Hellmann, and Feynman.

[42] E. Daniel and S.H. Vosko, Phys. Rev. **120**, 2041 (1960).

[43] S. Moroni, G. Senatore, and S. Fantoni, Phys. Rev. B **55**, 1040 (1997).

[44] W. Macke, Z. Naturforsch. A **5A**, 192 (1950).

[45] M. Gell-Mann and K.A. Brueckner, Phys. Rev. **106**, 364 (1957).

[46] L. Onsager, L. Mittag, and M.J. Stephen, Ann. Phys. (Leipzig) **18**, 71 (1966).

[47] J.C. Kimball, J. Phys. A **8**, 1513 (1975).

[48] H. Yasuhara and Y. Kawazoe, Physica A **85**, 416 (1976).

[49] D.J.W. Geldart, Can. J. Phys. **45**, 3139 (1967).

[50] J.C. Kimball, Phys. Rev. B **14**, 2371 (1976).

[51] Comparison of Eq. (A2) with Eq. (5) shows that RPA fails to reproduce the correct large-k expansion of $n(k,r_s)$: for small r_s, instead of having $k^8 n(k) \to \frac{8}{9}\pi^2(\alpha r_s^2)[\frac{1}{2}+O(r_s)]$, RPA yields $k^8 n(k) \to \frac{8}{9}\pi^2(\alpha r_s^2)[1+O(r_s)]$. The lowest-order exchange diagram (Ref. 48) repairs this, see Figs. 1(c) and 1(f) of Ref. 24.

[52] D. Pines and P. Nozières, *Theory of Quantum Liquids* (Benjamin, New York, 1966).

[53] R. Sartor and C. Mahaux, Phys. Rev. C **21**, 1546 (1980).

[54] G. Ortiz, M. Harris, and P. Ballone, Phys. Rev. Lett. **82**, 5317 (1999).

[55] M. Seidl, J.P. Perdew, and S. Kurth, Phys. Rev. A **62**, 012502 (2000); Phys. Rev. Lett. **84**, 5070 (2000).

[56] F.H. Zong, C. Lin, and D.M. Ceperley, Phys. Rev. E **66**, 036703 (2002).

[57] P. Ziesche, Int. J. Quantum Chem. **56**, 363 (1995).

[58] P. Ziesche, J. Mol. Struct.: THEOCHEM **527**, 35 (2000), and references therein. Therein factors 1/2 are erroneously incorporated in the definition of $g_{\uparrow\uparrow}(x)$ and $g_{\uparrow\downarrow}(x)$, such that $g_{\uparrow\uparrow}(\infty) = g_{\uparrow\downarrow}(\infty) = 1/2$ instead of 1.

[59] $s(0)=0$ together with the Macke formula $\epsilon_{\rm corr}(r_s \ll 1) = 0.062\,18 \ln r_s + \cdots$ obviously contradicts Collins' conjecture ''correlation entropy is of the order of magnitude of correlation energy'' (Refs. 57 and 60).

[60] D.M. Collins, Z. Naturforsch., A: Phys. Sci. **48**, 68 (1993).

[61] M.B. Ruskai, J. Math. Phys. **11**, 3218 (1970); K. Yasuda, Phys. Rev. A **63**, 032517 (2001).

[62] J.C. Kimball, Phys. Rev. A **7**, 1648 (1973).

[63] P.-O. Löwdin, Adv. Chem. Phys. **2**, 207 (1959).

[64] N. Iwamoto, Phys. Rev. A **33**, 1940 (1986).

[65] P. Ziesche, in *Electron Correlations and Materials Properties*, edited by A. Gonis, N. Kioussis, and M. Ciftan (Kluwer/Plenum, New York, 1999), p. 361.

[66] P. Ziesche, J. Tao, M. Seidl, and J.P. Perdew, Int. J. Quantum Chem. **77**, 819 (2000).

[67] K. Fuchs, Proc. R. Soc. London, Ser. A **151**, 585 (1935).

[68] R.A. Coldwell-Horsfall and A.A. Maradudin, J. Math. Phys. **1**, 395 (1960); **4**, 582 (1963).

[69] W.J. Carr, Jr., Phys. Rev. **122**, 1437 (1961).

[70] W.J. Carr, Jr., R.A. Coldwell-Horsfall, and A.E. Fein, Phys. Rev. **124**, 747 (1961).

[71] G. Diener, Diploma thesis, Dresden, 1961, cf. Ref. 74 p. 19.

[72] N.H. March and S. Sampanthar, Acta Phys. Hung. **XIV,** 61 (1962).

[73] P. Ziesche and G. Paasch, in *Ergebnisse in der Elektronentheorie der Metalle*, edited by P. Ziesche and G. Lehmann (Akademie/Springer, Berlin, 1983).

[74] A.K. Rajagopal, J.C. Kimball, and M. Banerjee, Phys. Rev. B **18**, 2339 (1978).